Label-free chemically specific imaging in planta with stimulated Raman scattering microscopy

Mansfield JC[1], Littlejohn GR[2], Seymour MP[3], Lind RJ[3], Perfect S[3], Moger J[1].

[1]School of Physics, University of Exeter, Exeter, EX4 4QL

[2]School of Biosciences, University of Exeter, Exeter, EX4 4QD

[3]Syngenta, Jealott's Hill International Research Centre, Bracknell, Berkshire, RG42 6EY

ABSTRACT: The growing world population puts ever-increasing demands on the agricultural and agrochemical industries to increase agricultural yields. This can only be achieved by investing in fundamental plant and agrochemical research and in the development of improved analytical tools to support research in these areas.

There is currently a lack of analytical tools that provide non-invasive structural and chemical analysis of plant tissues at the cellular scale. Imaging techniques such as coherent anti-Stokes Raman scattering (CARS) and stimulated Raman scattering (SRS) microscopy provide label-free chemically specific image contrast based on vibrational spectroscopy. Over the past decade these techniques have been shown to offer clear advantages for a vast range of biomedical research applications. The intrinsic vibrational contrast provides label-free quantitative functional analysis; it does not suffer from photobleaching; and allows near real-time imaging in 3D with submicron spatial resolution. However, due to the susceptibility of current detection schemes to optical absorption and fluorescence from pigments (such as

chlorophyll) the plant science and agrochemical research communities have not been able to benefit from these techniques and their application in plant research has remained virtually unexplored.

In this paper we explore the effect of chlorophyll fluorescence and absorption in CARS and SRS microscopy. We show that with the latter it is possible to use phase-sensitive detection to separate the vibrational signal from the (electronic) absorption processes. Finally we demonstrate the potential of SRS for a range of in planta applications by presenting in-situ chemical analysis of plant cell wall components, epicuticular waxes, and the deposition of agrochemical formulations onto the leaf surface.

KEYWORDS:

Stimulated Raman scattering, Coherent anti-Stokes Raman scattering, two-photon fluorescence, two photo-absorption, agrochemical, pesticide, herbicide, fungicide, plant biology

INTRODUCTION

Although resources devoted to plant biology are modest in comparison to biomedical research, plant biology will play a crucial role in ensuring the future of mankind. Basic plant biology and its application will be a major vehicle through which we will insure we can feed the increasing population, improve human health, meet increasing energy needs and provide a source of sustainable cost-effective materials. Of these challenges food security is the most prominent. With a rapidly growing world population, increased demand for high quality foods and also biofuels the pressure on agriculture to produce enough food is ever increasing. This is exacerbated by the loss of agricultural land due to erosion and climate. Improved plant

breeding and crop protection is needed to meet these challenges and this can only come through fundamental plant science and agrochemical research.

A major challenge in plant and agrochemical research is to measure heterogeneity in chemical composition at the sub-cellular scale. Hence there is a clear need to develop improved high-resolution, non-destructive, analytical techniques for that provide quantitative microanalysis of both cellular structure and chemical composition in live plant tissues. Having the ability to map chemical composition in this way would represent a major advance in research capability across all areas of plant science; spanning fundamental plant biology; crop science; industrial biotechnology; agrochemical research and biofuel production.

Techniques based on vibrational spectroscopy provide in-situ chemical analysis derived from the vibrational frequencies of molecular bonds. However, due to water absorption and the intrinsically low spatial resolution associated with the long infrared wavelengths required to directly excite molecular vibrations infrared absorption techniques have limited value for bio-imaging. Raman scattering however, provides analysis of IR vibrational frequencies by examining the inelastic scattering of visible (or near IR) light. The Raman scattered light is frequency shifted with respect to the incident light by discrete amounts which correspond to molecular vibrational frequencies. However, Raman scattering is a weak effect with typical photon conversion efficiencies in biological materials of the order of 1 in 10^{10}. This limits the in vivo applications of Raman since long acquisition times (100ms to 1s per pixel) at relatively high excitation powers are required to detect most biomolecules with sufficient sensitivity. However novel techniques involving multiple foci have the potential to reduce imaging times[1]. This lack of sensitivity is compounded by the susceptibility of Raman

scattering to interference from autofluorescence, which overwhelms the Stokes-shifted light and virtually prohibits its application in living plant tissues.

Far stronger Raman signals can be obtained using coherent Raman scattering (CRS)[2]. CRS achieves a signal enhancement by focusing the excitation energy onto a specific Raman mode. Pump and Stokes beams, with frequencies ω_p and ω_s respectively, are incident upon the sample with the frequency difference $\omega_p - \omega_s$ chosen to match the molecular vibrational frequency of interest. Under this resonant condition bonds are coherently driven by the excitation fields and a strong non-linear coherent Raman signal is produced. When applied in microscopy format CRS benefits from the non-linear nature of the process which confines the signal to the focal spot (which is typically sub-micron for high numerical aperture objectives) that can be scanned in space, allowing three-dimensional mapping of bio-molecules with sub-micron resolution. Near-IR excitation wavelengths can be employed which reduce photodamage and increase depth penetration into scattering tissues; since the CRS process does not leave sample molecules in an excited electronic state it does not suffer from photobleaching.

CRS was first introduced as a microscopic technique by Duncan et al in 1982[3] in which coherent anti-Stokes Raman scattering (CARS) was shown to provide vibrational imaging of biological samples. When these techniques were combined with more practical ultra-fast IR laser systems by Zumbusch et al in 1999[4] its potential for a highly sensitive imaging technique was realized. CARS imaging uses the anti-Stokes signal generated at frequency $\omega_{as} = 2\omega_p - \omega_s$, which is spectrally isolated from the pump and Stokes beams to map the location of biomolecules of interest. Over the past decade significant research activity has focused on the technical refinement of CARS microscopy which has allowed in-vivo imaging of neurons in rodents[5], embryogenesis in zebrafish[6], and skin[7]. Despite the great potential of CRS as an analytical imaging tool for plant biology, very little work has been published in

this area. This is due to the extremely strong optical absorbance and autofluorescence in plants which makes chemically specific imaging with CRS extremely challenging. The autofluorescence from plants enables high resolution structural imaging, but with a wide range of fluorophores emitting at the similar wavelengths this data is not chemically specific. In spontaneous Raman and coherent anti-stokes Raman the chemically specific information from the molecular bond vibrations is weaker than the fluorescence. Therefore most successful CARS studies on plants have focused on structures away from the main sources of fluorescence for example dried stems[8], plant roots[9], bulbs[3] tubers and fruits[10] and waxes striped away from the leaf surface[11]. Frequency modulated coherent Raman techniques are more promising for imaging in planta and the applications of this have been demonstrated with stimulated Raman scattering in stems[12] and frequency modulated CARS in corn leaves[13].

Stimulated Raman Scattering (SRS) has recently been reported as alternative CRS technique that relies on detecting subtle changes in the intensities of the excitation fields that occur by virtue of stimulated excitation[14,15]. When the difference frequency, $\omega_p - \omega_s$, matches a molecular vibrational frequency the intensity of the Stokes beam, I_S, experiences a gain, ΔI_s, while the intensity of the pump beam, I_p, experiences a loss, ΔI_p. The intensity transfer from the pump to the Stokes beam only occurs when both beams are incident upon the sample and can be detected with high sensitivity using modulation transfer detection. Modulating the intensity of either the pump or Stokes beam modulates the SRS process and can be detected as gain (Stimulated Raman Gain, SRG) in the Stokes beam or a loss in the pump beam (Stimulated Raman Loss, SRL). The amplitude of the transferred intensity modulation is directly proportional to the concentration of target molecules and by

modulating at frequencies above laser noise (>1 MHz) the signal can be detected with a lock-in amplifier with great sensitivity (1 in 10^6 photons)[16].

Since SRS is detected at the same wavelength as the excitation fields it is not affected by fluorescent emission, however, SRS can succumb to interference from strongly absorbing compounds. Single- or two- photon electronic absorption of either the pump or Stokes beams, despite reducing their intensity, does not produce a modulation transfer between the beams since there is no temporal correlation between the absorption of the different wavelengths and therefore does not interfere with the SRS signal. However, two-color two-photon absorption (TPA) of the combined pump and Stokes beams does result in modulation transfer since their combined absorption can only occur when both beam are incident upon the sample. In most samples this is a weak effect, however in plant tissues the optical absorption is sufficiently strong across a broad spectral range and TPA overwhelms the SRS signal. Figure 1 shows a schematic of the CARS, SRS and TPA processes and their effect on the detected intensity transfer.

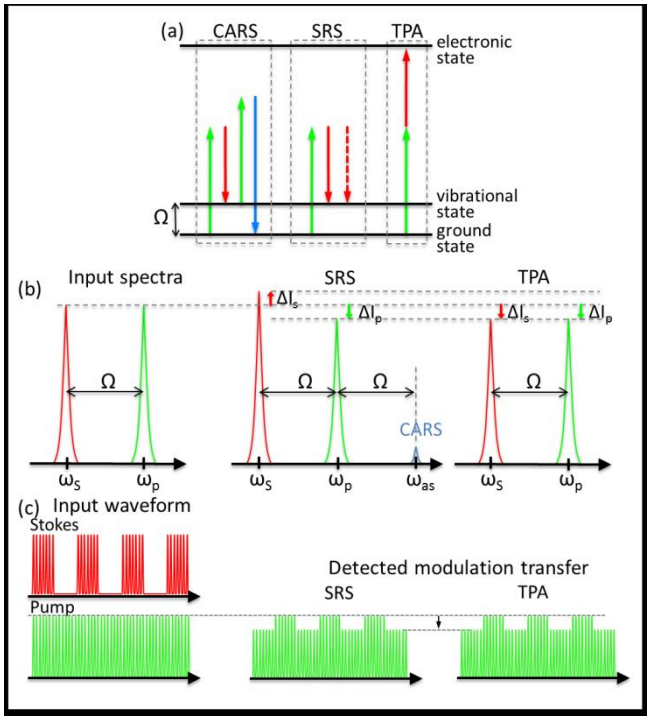

Figure 1: Schematic illustration of the CARS and TPA processes. (a) shows the energy level diagram for CARS, SRS and TPA, (b) the input and output spectra of the three processes, and (c) the detected modulation transfer signals for SRS and TPS.

In this paper we explore the issues associated with performing CRS in planta by comparing the origin of the background signals that hinder both CARS and SRS imaging. We show that with the latter it is possible use phase-sensitive detection to separate the vibrational signal from the (electronic) absorption processes. Finally we demonstrate the potential of SRS for a range of in planta analysis applications by presenting in-situ analysis of plant cell wall components, epicuticular waxes, and the deposition of agrochemicals onto the leaf surface.

METHODS:

Multimodal Non-linear Optical Microscopy

Laser sources:

A combination of two laser systems were used for coherent Raman excitation. The first system was comprised of a Nd:Vanadium pico-second oscillator at 1064nm (picoTrain highQ

laser) and an OPO (Levante Emerald, APE) which was pumped by the frequency doubled output of the picoTrain laser. This system was used for CARS and SRL where the 1064nm output from picoTrain laser was used as the Stokes beam and the signal from the OPO was used as the pump beam. For SRL Stokes beam was modulated at 1.7MHz using an electro optical modulator (EOM) (Leysop EM200). For SRG a Ti:Sapphire laser (Mira, coherent) operating in pico-second mode at 770nm was used as the pump beam. The pump beam was modulated at 1.7MHz using an acoustic optical modulator (AOMO 3080-122 Crystal Technology) and 80MHz driver (AODR 1080AF-A1F0-1.0, Crystal Technology). The signal output from the pico-second OPO was used as the Stokes beam, this was tunable to allow different Raman shifts to be accessed. The pump and Stokes beams were collimated on separate telescopes and then combined at an 850nm short pass dichroic filter. The Ti:Sapphire laser was locked to the picoTrain laser via electronic synchronization (Synchrolock, Coherent). The optical table set-up is summarized in figure 2.

Microscopy:

All imaging was carried out on a modified con-focal laser scan unit (Flouview 300 Olympus) and an inverted microscope (IX71 Olympus). This system was capable of CARS, TPF, SHG and SRS imaging and was also coupled to a spectrometer to allow micro-spectrometry. The light was focused onto the sample using a 60X 1.2NA water immersion microscope objective (UPlanSApo, Olympus).

SRS was detected in the forwards direction using a Si photodiode (FDS1010 thorlabs) with a 70V reverse bias. The forward propagated light was collected using a 100X 1.4NA oil immersion microscope objective (UPlanSApo, Olympus) for thin samples and a 60X 1.0NA water immersion (LUMFI, Olympus) microscope objective for thicker samples. To suppress the strong signal due to the laser pulsing at 76MHz, the output current was filtered by a low pass filter (mini-circuits, BLP-1.9+) and then terminated by a 50Ω resistor. The photo-diode

was connected to a radio frequency lock-in amplifier (Zurich instruments, HF2L1 Lock-in amplifier) which detected the modulations in the at the 1.7MHz frequency. This allowed both the amplitude and the phase of the modulations to be recorded. A 100μs integration time was chosen on the lock-in amplifier and this resulted in a 13s frame rate for 256x256 pixel images and a 53s frame rate for 512x512 pixel images. For SRG the pump beam was blocked from the photodiode by an 850nm long pass filter (hq850lp) and the Stokes beam was detected allowing Raman shifts from 1200-3000cm^{-1} to be probed. For SRL the Stokes beam was blocked with a band pass filter (CARS 890/220nm, Chroma technologies) and the pump beam was detected.

CARS or TPF images were simultaneously detected in the epi-direction using a 750nm long pass dichroic (750dcxr Chroma) and two filters centered at 660nm (660.0 IF 40D Ealing Inc) to separate the signal from the laser fundamental.

Spectra were acquired using a spectrograph (Andor Technology shamrock sr-303i) and a CCD camera (Andor Technology IDUS) cooled to -65°C with a 150 l/mm grating with a blaze at 800nm. The light was collected in the epi direction and to block any laser fundamental from reaching the CCD camera filters were placed in front of the spectrometer. Spectra were taken using a variety of excitation wavelengths that corresponded to those used to excite for coherent Raman scattering.

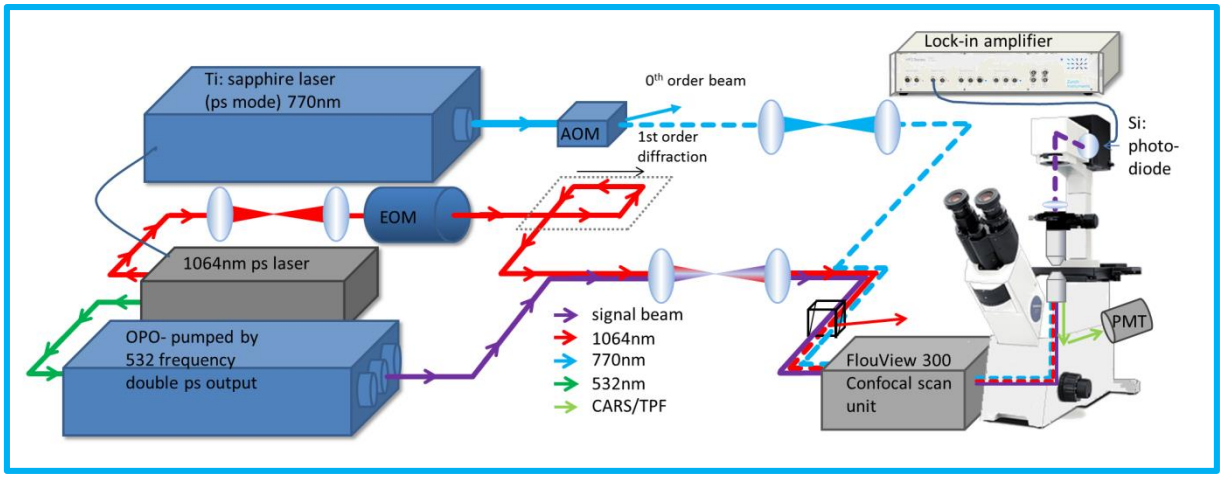

Figure 2. A schematic diagram of the imaging system for coherent Raman. For SRL imaging the pump beam is the signal from the OPO and the Stokes beam is 1064nm. For SRG imaging the pump beam is 770nm and the stokes beam is the signal beam from the OPO

Spontaneous Raman

Spontaneous Raman spectra were obtained for selected agrochemicals, their formulations and purified plant components using a Renishaw RM1000 Raman Microscope (Renishaw plc, UK). This contained a 785nm diode continuous wave laser with a maximum power at the sample of 300mW and a spectral grating with 1200 lines/mm which gave a spectral resolution of 1 cm^{-1}.

Sample preparation

Maize (*Zea mays*) and cotton (*Gossypium hirsutum*) plants were propagated in a green house. Three agrochemicals were investigated in this study chlorothalonil, azoxystrobin and deuterated glyphosate. Azoxystrobin and chlorothalonil were prepared in a solution of 1mg/ml in a solvent of 20:80 acetone: water with 0.05% Tween. Deuterated glyphosate was prepared at a concentration of 100mg/ml in an aqueous solution with 7% tallow amine formulation. A series of 20 0.5µl droplets of each of the prepared solutions were applied to the adaxial leaf surface. The leaves were treated 24hrs prior to imaging for azoxystrobin and chlorothalonil and 30minutes prior to imaging for deuterated glyphosate. For imaging, the

leaves were mounted between 2 coverslips using perfluorocarbon as a mounting medium[17]. The concentrations of azoxystrobin and chlorothalonil used here are comparable to some typical field rates 1 mg/ml and 3 mg/ml respectively. The concentration of deuterated glyphosate was approximately 20X higher than the typical field rate.

RESULTS:

To illustrate how autofluorescence prohibits CARS microscopy in planta figures 3A-C show images of a cotton leaf. When either the pump or Stokes beams are blocked a strong TPF signal remains, indicating that the image is dominated by autofluorescence and contains virtually no vibrational data.

Emission spectra of the autofluorescence excited using both the pump and Stokes beams (figure 3E) confirm the spectral overlap with the CARS emission. The strong peaks at 680 and 730nm correspond to chlorophyll fluorescence[18,19]. The fluorescent emission is sufficiently intense that no anti-Stokes signal (expected at 660nm corresponding to CH vibrations) can be seen. Figure 3F shows that additional weaker fluorescence was also detected from the chloroplasts at 550-600nm (attributed to β- carotene, riboflavin, FAD and FMN[19]) and from the leaf hairs and cell walls at around 500nm (attributed to hydroxycinnamic acids[20] or ferulic acid[21]). Due to the narrow band nature of the anti-Stokes signal the relative contribution of the broad band TPF signal can be reduced by applying a narrow band pass filter, however this cannot completely separate out the TPF signal and also complicates tuning between different Raman bands.

The autofluorescence covers a broad spectral range making it challenging to find a window in which to carry out CARS imaging. If shorter pump and Stokes wavelengths are chosen the anti-Stokes signal will no-longer overlap with the chlorophyll emission, however the other

fluorophores identified in figure 3F will cause interference. On the other hand, if the anti-Stokes wavelength is greater than 800nm then in principle it could be isolated from background fluorescence, however when imaging at the longer wavelengths water absorption can become a problem as imaging Raman shifts in the CH vibration region will require a Stokes beam greater than 1500nm.

Figure 3D shows an SRL image acquired simultaneously with the CARS images. Since stimulated Raman is detected as a change in intensity of the pump or Stokes beams, which are spectrally distinct from the two-photon excited autofluorescence, no background autofluorescence is observed. Here the cell walls are clearly delineated based on the CH stretching modes. The cell wall signal is shown to vary with $\omega_p - \omega_s$ (fig 4A), moreover, when $\omega_p - \omega_s$ is tuned away from the CH Raman band the signal disappears, which is consistent with the background-free purely vibrational response indicative of SRS. The chloroplasts also feature strongly in figure 3D, however, despite being rich with CH bonds, they exhibit virtually no spectral dependence.

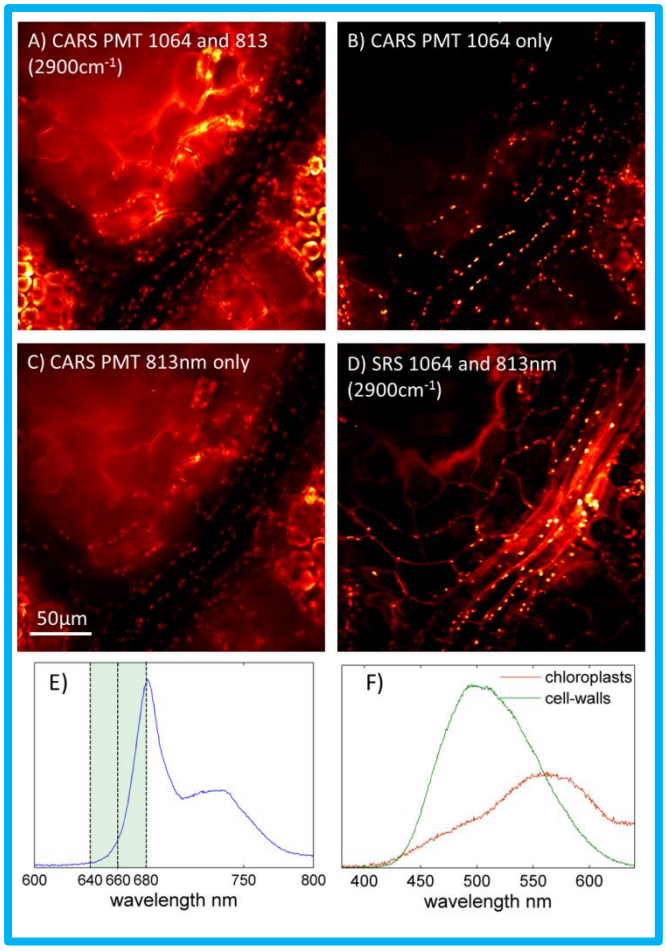

Figure 3. A-C) images of a cotton leaf taken with the CARS PMT (emission filter 660nm 40nm FWHM) with laser excitation from A) both pump and Stokes beams, B) Stokes beam only and C) pump beam only. D) SRS image of the same area (when pump or Stokes beam were blocked the signal disappeared (data not shown)) E) Fluorescence spectrum of chloroplasts excited by a combination of 813 and 1064nm pump and Stokes beams. (Here the green shaded area indicates the transmission range of the filters used for CARS imaging) F) fluorescence from cell walls and chloroplasts at shorter wavelengths (excited by 813nm light)

To investigate the origin of the non-vibrational contrast from the chloroplasts in the SRL channel it is useful to examine the phase of the signal with respect to the amplitude modulation of the Stokes beam and its dependence on excitation power. Figure 4B shows that the chloroplast signal is in phase with the SRL signal in the cell walls, indicating that the origin of this signal is also a loss process. The chloroplast signal followed a linear power

dependence for both the pump and Stokes beams (figure 4C and D) which follows the expected trend for a two-color two-photon absorption (TPA) process[16].

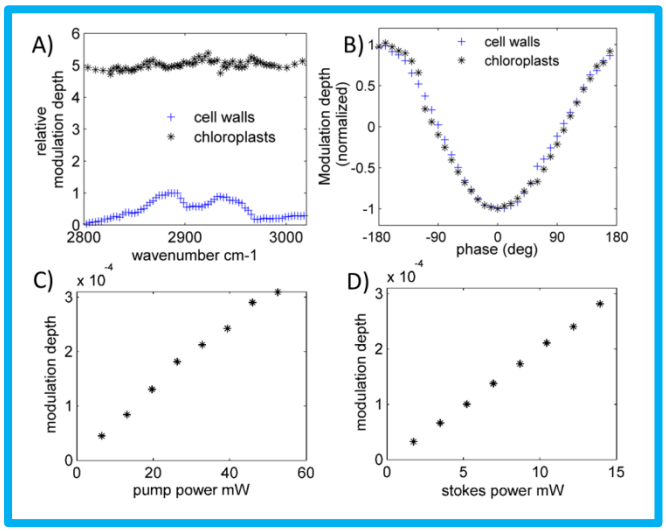

Figure 4. TPA and SRL in planta excited using pump and Stokes beam 813 and 1064nm A) spectra from the cell walls and the chloroplasts (the cell walls show a strong spectral dependence, whereas the signal from the chloroplasts shows little spectral dependence) B) Phase of chloroplast and cell wall signals (referenced to the modulation phase of the Stokes beam) C) power dependence of chloroplast signal on pump beam (Stokes beam kept constant at 17.5mW) D) power dependence of chloroplast signal on Stokes beam power (pump beam kept constant at 50mW)

Figure 5A) shows the phase of the signals from cell walls and the chloroplast measured using SRG. In this arrangement the chloroplast signal appears approximately 130^{o} out of phase from the cell wall signal. Two-color TPA, alone would appear at exactly 180^{o} to SRG since the processes manifest in a loss and gain of the Stokes beam respectively.

The discrepancy in phase can be explained by two-photon photothermal lensing (TPPL)[22,23]. Local heating resulting from resonant two-photon absorption of the pump beam causes a refractive index gradient, which results in a deflection of the probe (in this case the Stokes) beam that is detected as a loss in intensity. Although TPPL produces as loss in the probe intensity, the thermal gradient builds up during pulses resulting in a peak signal that

does not necessarily occur in phase with the pump beam modulation. The phase delay between the pump and probe is dependent on modulation frequency and the thermal properties of the sample and can in principle produce an arbitrary phase shift in the loss signal.

To confirm the presence of TPPL the chloroplast signal was measured when the pump and Stokes beams were desynchronised. For both SRL and SRG some signal remained when the beams were no longer temporally overlapped. Two-color TPA requires the beams to be temporally overlapped however degenerate two-photon photothermal lensing can still occur when the beams are desynchronized. The signal detected in the absence of a temporal overlap must therefore be due to photothermal effects. The photothermal effects are much stronger for SRG compared to SRL (this is indicated by the large phase shift seen in figure 5A). This is due to were the two-photon absorption wavelengths of the modulated beams fall on the absorption spectrum of chlorophyll. For SRL the modulated beam (1064nm) corresponds to 532nm where the absorption of both chlorophyll a and b is weak, however for SRG the modulated beam (770nm) corresponds to absorption at 385nm which is close to a peak in the absorption of chlorophyll a.

Mapping the modulus and the phase of the SRG channel (figure 5B and 5C respectively) provides a useful visualization of the differences in signal origin from different leaf components. Figure 5C clearly highlights the difference in phase between the chloroplasts and cell walls. It shows a range of different phases in the chloroplast signal, indicating that the ratio of TPPL to TPA differs between individual chloroplasts. This may relate to difference in the ratio of chlorophyll a:b. The peak of absorption of chlorophyll a is blue shifted with respect to chlorophyll b. Consequently the two-photon absorption of the pump (at 385nm) will be strong for chlorophyll a but very weak for chlorophyll b[24]. Therefore a

relative increase in the ratio of chlorophyll a:b will result in increased TPPL and an increase in temporal lag. Combining the modulus and phase data enables image contrast to be generated at any specified phase and by selecting phases corresponding to SRG and TPA/TPPL enables the chloroplast and the coherent Raman signal to be separated as shown in figures 5D-F.

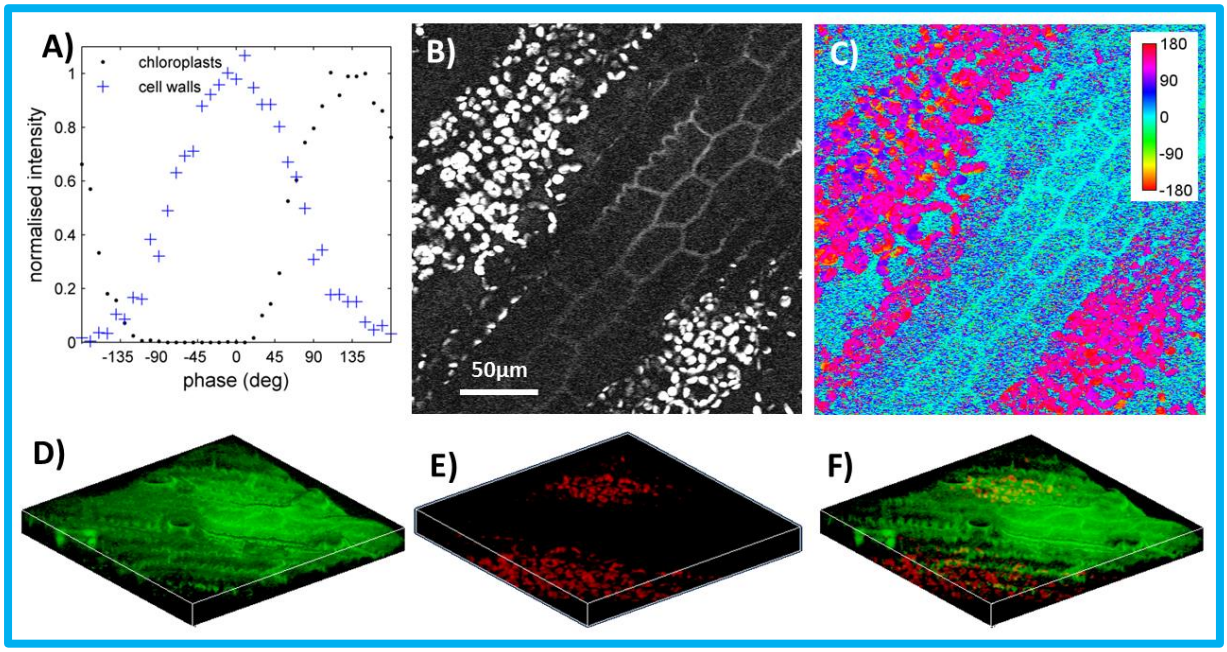

Figure 5. The use of phase to separate SRG and TPA. A) phase dependence of chloroplast signal and the SRG from the plant cell walls. B) and C) Images showing the modulus (R) and the phase of the signal for a maize leaf. D-F) 3D reconstructions of a maize leaf showing how the SRG and the TPA signal can be separated by phase sensitive imaging. D) SRG from the CH vibration in the cell walls and E) TPA from the chloroplasts. F) merged image showing SRG (green) and TPA (red)

Chemically-specific structural imaging and analysis in planta

To exemplify the use of SRS for fresh plant tissues on the cellular scale, we performed structural and chemical analysis of epicuticular waxes and cell walls. Understanding the structural and chemical composition of cuticle waxes is of particular interest to agrochemical applications as both the epicuticular wax and the cell walls are barriers which agrochemicals

must cross in order to enter the plant. They also provide much of the plant's natural defenses against pathogens and disease. Microscopic chemical analysis of the cell wall composition has a wide variety of plant biology applications ranging from fundamental questions relating to plant growth and biochemical response to pathogens and commercial R&D applications such as fiber processing for the biofuel and materials industry.

Figure 6A-D) shows SRL images and spectra of cell walls acquired over the CH region of maize and cotton. The SRL spectra are overlaid with the spontaneous Raman spectra of cellulose and pectin (major components of the cell wall). The principle spectral components correspond to those in current literature[25,26]. Analysis of the SRL spectra acquired from the cell wall provides an indication of the composition and from figure 6C and D it can clearly be seen to differ between the two crop plants investigated.

The epicuticular waxes again gave a strong signal in the CH region with a strong peak at 2840cm^{-1} from the symmetric CH_2 stretch and an even stronger peak at 2870cm^{-1} from the anti-symmetric CH_2 stretch (see figure 6H). To provide complementary data on both the cell walls and waxes images were taken at both 2840cm^{-1}(figure 6F) and 2930cm^{-1} (figure 6E). At 2930cm^{-1} only the cell walls are visible however at 2840cm^{-1} the wax crystals appear. Imaging at these two wavenumbers enables these two chemically different structures to be identified.

Another important component of some plant cell walls is lignin, which is primarily found in the stems and woody parts of plants but also in the xylem vessels within the leaf veins. Lignin has a strong Raman mode at ~1600cm^{-1} which is attributed to –C=C- stretching in the phenyl groups[8,12,26]. Using SRL we are able to image the lignin distribution at a leaf vein (figure 6 I-K). The image taken at 2930cm^{-1} shows the structure of the cell walls in the leaf vein and surrounding tissue; whereas the image taken at 1600cm^{-1} shows that the lignin is localized within the leaf vein.

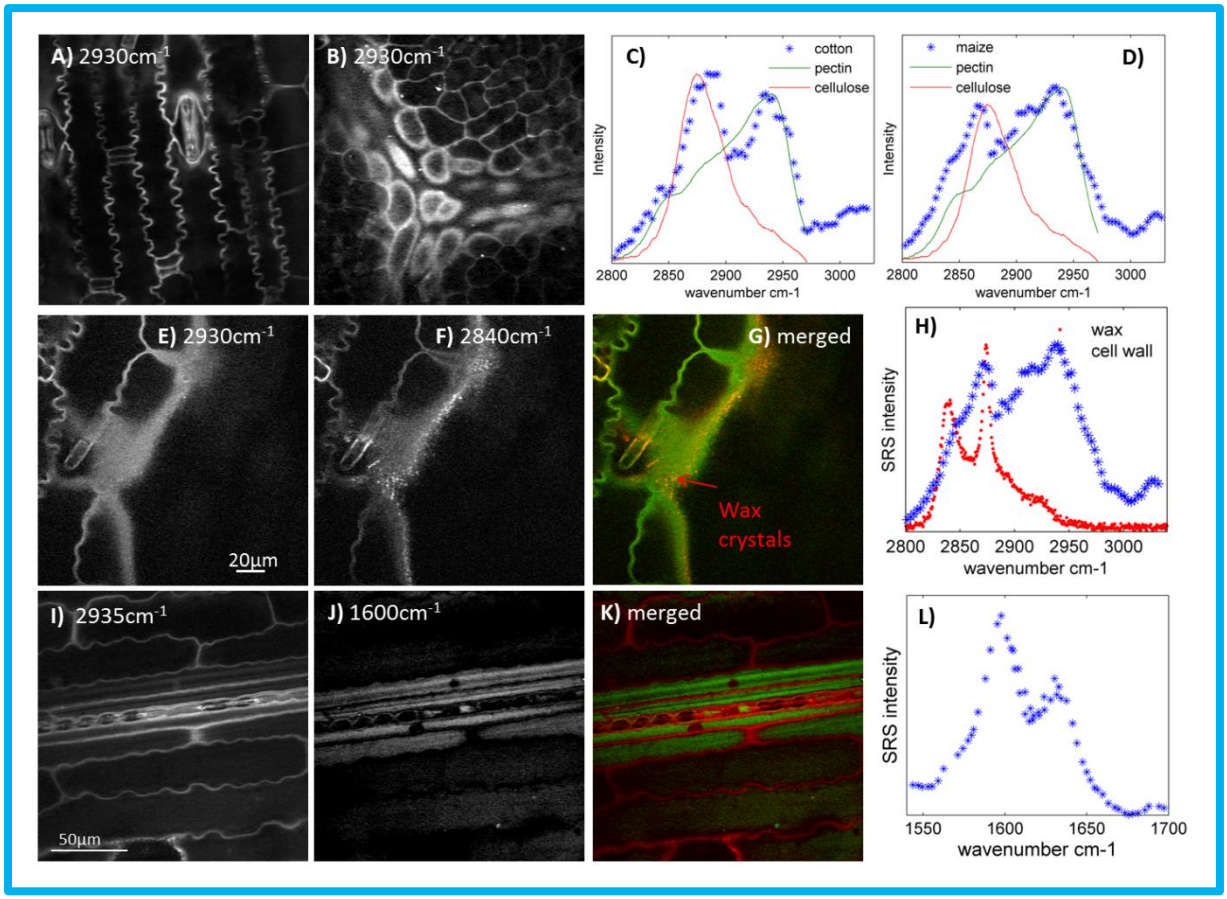

Figure 6. SRL imaging provides structural and chemically specific information on untreated leaves. A) and B) images of cells walls in the upper epidermis of maize and cotton taken from the spectra data set at 2930cm^{-1}. C) and D) the SRL spectra of cotton and maize over the CH region overlaid with the spontaneous Raman of cellulose and pectin (SRL spectra are acquired from the entire field of view). E-G) images of the surface of a maize leaf taken at 2930cm^{-1} and 2840cm^{-1} giving contrast for the cell walls and waxes respectively (in merged image 2930cm^{-1} is green and 2840cm^{-1} is red). H) Spontaneous Raman of purified wax from a maize leaf overlaid on the spectra of maize cell walls. I-K) Imaging of vascular bundles in a maize leaf vein at the 2930cm^{-1} CH_3 vibration and the phenyl stretching vibration at 1600cm^{-1} (in merged image 2935cm^{-1} is red and 1600cm^{-1} is green). L) SRL spectra of the lignin peak around 1600cm^{-1} (acquired from the central region of image6J).

Agrochemical Imaging

To demonstrate the potential application of SRS as an analytical tool for the agrochemical industry we investigated the deposition and uptake of two commercially available fungicides azoxystrobin and chlorothalonil. Both these compounds, like many agrochemicals, contain

C≡N groups which give rise to a strong Raman band in the so-called *silent region* which is devoid of naturally found resonances and facilitates their detection within biological tissues (see figure 7A). The C≡N peak position differed slightly between the two compounds reflecting differences in molecular composition and was found to be at 2225cm^{-1} and 2234cm^{-1} for azoxystrobin and chlorothalonil respectively. These were significant enough to enable us to differentiate chemically between the compounds with SRL imaging as shown in figure 7B. SRL was used to image leaves treated with each of these fungicides and this revealed crystalline deposits of the chemical on the leaf surface. The C≡N vibration was used to visualize the agrochemical crystals and the CH_3 vibrations at 2930cm^{-1} gave structural information on the cell walls.

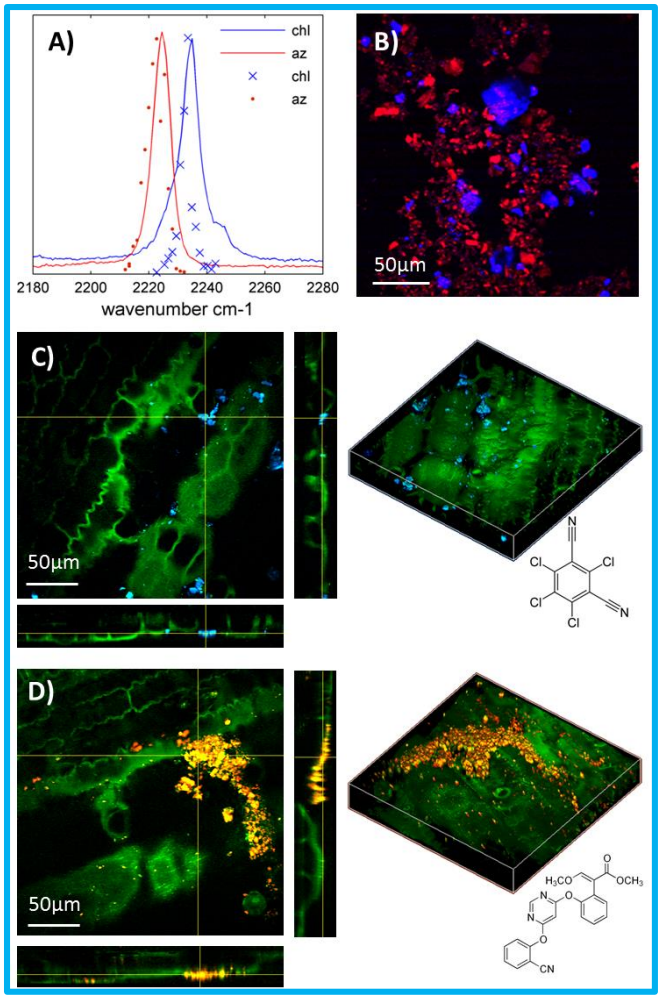

Figure 7. Two fungicides azoxystrobin (az) and Chlorothalonil (chl) applied to maize leaves. A) SRL and spontaneous Raman of azoxystrobin and chlorothalonil showing the C≡N peak, N.B. the peak is slightly different between the 2 chemicals (2225cm^{-1} for Azoxystrobin and 2234cm^{-1} for chlorothalonil) B) SRL Image of a mixture of AZ and CHL showing that we are chemically specific between the 2 AIs (here red is AZ imaged at 2225cm^{-1} and blue is CHL imaged at 2234cm^{-1}) C) Chlorothalonil applied to a maize leaf (blue = SRL at 2234cm^{-1} from the C≡N bond, green =SRL at 2930cm^{-1} from the CH_3 vibrations) D) Azoxystrobin applied to a maize leaf (red = SRL at 2225cm^{-1} from the C≡N bond, green =SRL at 2930cm^{-1} from the CH_3 vibrations) (note that in this section the azoxystrobin crystals appear yellow/orange as contrast from both the CH bonds (green) and CN bond (red) has been combined

Many agrochemicals do not contain Raman vibrations within the silent region. To aid chemically specific imaging of these compounds deuterium labeling was investigated. Replacing hydrogen atoms with heavier deuterium replaces the CH_2 band (~2850cm^{-1}) with the red-shifted CD_2 band (~2100cm^{-1}) situated in the silent-region and hence allowing similar

spectral isolation from biological tissues as the CN band. Since deuterated compounds have been shown to exhibit comparable transport and uptake as their non-deuterated counterparts[27,28] this technique has great potential as a suitable 'label' for studying transport kinetics[29,30]. We applied deuterium labeling to the widely used herbicide glyphosate. This introduced C-D vibrational peaks at 2164cm^{-1}, 2214cm^{-1} and 2248cm^{-1} (see figure 8A and B). Glyphosate is often applied within a formulation that aids its transfer across the waxy cuticle. The Raman spectrum of one such formulation matrix (shown in figure 8D) exhibited a strong contribution from the CH_2 symmetric stretch at 2850cm^{-1} enabling SRG to easily differentiate between the deuterated glyphosate, the plant structures and formulation (shown in figures 8E). At 2850cm^{-1} the rectangular crystal appears darker than the surrounding formulation, some SRG signal is detected from the crystal as it is not fully deuterated. At 2164cm^{-1} there is SRG signal from the crystal along with additional signal from the formulation and the edge of the formulation. This suggests that there is some deuterated glyphosate dissolved within the formulation and possible glyphosate re-crystallization on the formulation surface. In figure 8C the plant cell walls are visualized using TPF. When imaging with shorter wavelengths this strong signal provides an alternative to SRS for the complementary structural imaging and may be preferable as it allows faster imaging speeds.

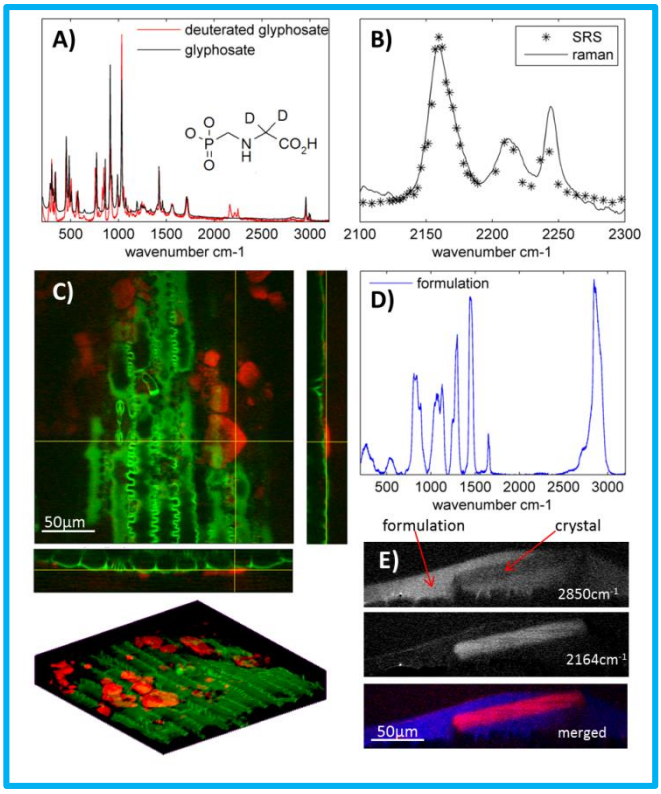

Figure 8. Deuterated Glyphosate application with formulation onto maize leaves. A) spontaneous Raman spectrum of deuterated and non-deuterated glyphosate showing the peaks generated in the silent region by deuteration (inset shows the Hydrogen atoms within the molecule which have been replaced with deuterium) B) SRG spectra of the C-D peaks in the deuterated glyphosate. C) Deuterated gylphosate crystals on a maize leaf (red = glyphosate, green = cell walls (TPF). D) spontaneous Raman spectrum of glyphosate formulation showing a very strong peak at 2850cm^{-1} corresponding to CH vibrations in aliphatic chains. E) imaging deuterated glyphosate (2164cm^{-1}) and formulation (2850cm^{-1}) applied to leaves in the merged image blue = 2850cm^{-1} and red = 2164cm^{-1}.

CONCLUSIONS

There is a clear need for techniques that combine structural imaging with in-situ chemical analysis of plant materials with sub-cellular spatial resolution, and in this paper we propose that coherent Raman scattering offers a solution. We have demonstrated that while CARS microscopy in living plants is prohibited by chlorophyll autofluorescence that spectrally overlaps the anti-Stokes signal, the modulation transfer detection scheme used for SRS

imaging is not affected. SRS does however suffer from two-photon absorption of the combined pump and Stokes beams and that for shorter pump wavelengths, two-photon absorption of the pump beam causes interference due to photothermal lensing. We have shown that with phase-sensitive detection of the SRG signal it is possible to separate the chemically specific SRS signal from the TPA and TPPL. Moreover, the relative phases of the TPA and TPPL themselves proved useful information regarding the specific type of chlorophylls present within plant cells. We exemplified the utility of the technique for performing in-situ structural and chemical analysis in living plant tissues by performing both structural and chemical analysis of plant cell walls and epicuticular waxes and to image a range agrochemicals and formulation compounds on fresh plant leaves. Performing spectral scans or tuning between specific wavelengths allowed us to identify between different chemical compounds.

The in planta imaging applications reported in this study represent only a small fraction of the potential areas in which SRS could be applied. It is anticipated that the simple detection and analysis technique reported here can be applied to a wide range of research applications in the plant sciences.

ACKNOWLEDGEMENTS

We would like to thank Jim Chadlow for propagating the plants and Ellen Green for her support in the biophysics laboratory. This work was funded by Syngenta.

ABREVIATIONS

SRS, stimulated Raman scattering; SRL, stimulated Raman loss; SRG, stimulated Raman gain; CARS, coherent anti-Stokes Raman scattering; CRS, coherent Raman scattering; TPA, two photon absorption; TPPL, two photon photothermal lensing.

REFERENCES

(1) M. Okuno, H.-o. Hamaguchi, Opt. Lett., **2010**, 35, 4096-4098.

(2) C.L. Evans, X.S. Xie, Annual Review of Analytical Chemistry, **2008**, 1, 883-909.

(3) M.D. Duncan, J. Reintjes, T.J. Manuccia, Opt. Lett., **1982**, 7, 350-352.

(4) A. Zumbusch, G.R. Holtom, X.S. Xie, Physical Review Letters, **1999**, 82, 4142-4145.

(5) H.F. Wang, Y. Fu, P. Zickmund, R.Y. Shi, J.X. Cheng, Biophys. J., **2005**, 89, 581-591.

(6) A. Takesono, J. Moger, S. Faroq, E. Cartwright, I.B. Dawid, S.W. Wilson, T. Kudoh, Proc. Natl. Acad. Sci. U. S. A., **2012**, 109, 3371-3376.

(7) C.L. Evans, E.O. Potma, M. Puoris'haag, D. Cote, C.P. Lin, X.S. Xie, Proc. Natl. Acad. Sci. U. S. A., **2005**, 102, 16807-16812.

(8) Y. Zeng, B. Saar, M. Friedrich, F. Chen, Y.-S. Liu, R. Dixon, M. Himmel, X. Xie, S.-Y. Ding, BioEnergy Research, **2010** ,3, 272-277.

(9) S. Ly, G. McNerney, S. Fore, J. Chan, T. Huser, Opt. Express, **2007**, 15, 16839-16851.

(10) C. Brackmann, A. Bengtsson, M.L. Alminger, U. Svanberg, A. Enejder, Journal of Raman Spectroscopy, **2010**, 4, 586-592.

(11) I. Weissflog, N. Vogler, D. Akimov, A. Dellith, D. Schachtschabel, A. Svatos, W. Boland, B. Dietzek, J. Popp, Plant Physiology, **2010**, 154, 604.

(12) B.G. Saar, Y.N. Zeng, C.W. Freudiger, Y.S. Liu, M.E. Himmel, X.S. Xie, S.Y. Ding, Angewandte Chemie-International Edition, **2010**, 49, 5476-5479.

(13) B.C. Chen, J.H. Sung, S.H. Lim, Journal of Physical Chemistry B, **2010**, 114, 16871-16880.

(14) C.W. Freudiger, W. Min, B.G. Saar, S. Lu, G.R. Holtom, C.W. He, J.C. Tsai, J.X. Kang, X.S. Xie, Science, **2008**, 322, 1857-1861.

(15) P. Nandakumar, A. Kovalev, A. Volkmer, New Journal of Physics, **2009**, 11, 033026.

(16) T. Ye, D. Fu, W.S. Warren, Photochemistry and Photobiology, **2009**, 85, 631-645.

(17) G.R. Littlejohn, J.D. Gouveia, C. Edner, N. Smirnoff, J. Love, New Phytologist, **2010**, 186, 1018-1025.

(18) P.-c. Cheng, B.-L. Lin, F.-J. Kao, M. Gu, M.-G. Xu, X. Gan, M.-K. Huang, Y.-S. Wang, Micron, **2001** , 32, 661-669.

(19) F.-J. Kao, Y.-M. Wang, J.-C. Chen, P.-C. Cheng, R.-W. Chen, B.-L. Lin, Journal of Luminescence, **2002**, 98, 107-114.

(20) S. Meyer, A. Cartelat, I. Moya, Z.G. Cerovic, Journal of Experimental Botany, **2003**, 54, 757-769.

(21) C. Buschmann, H.K. Lichtenthaler, Journal of Plant Physiology, **1998**, 152, 297-314.

(22) S. Lu, W. Min, S. Chong, G.R. Holtom, X.S. Xie, Appl. Phys. Lett., **2010**, 96, 113701.

(23) J. Moger, N.L. Garrett, D. Begley, L. Mihoreanu, A. Lalatsa, M.V. Lozano, M. Mazza, A. Schatzlein, I. Uchegbu, Journal of Raman Spectroscopy, **2012**, 5, 668-674.

(24) G. Mackinney, J. biol. Chem, **1941**, 140, 315-322.

(25) A. Synytsya, J. Copikova, P. Matejka, V. Machovic, Carbohydrate Polymers, **2003**, 54, 97-106.

(26) U.P. Agarwal, S.A. Ralph, Applied spectroscopy, **1997**, 51, 1648-1655.

(27) Y.H. Lin, N. Salem, Journal of Lipid Research, **2007**, 48, 2709-2724.

(28) K. Akira, R.D. Farrant, J.C. Lindon, S.T. Caddick, A.W. Nicholls, J.K. Nicholson, Analytical Biochemistry, **1994**, 221, 297-302.

(29) N.L. Garrett, A. Lalatsa, D. Begley, L. Mihoreanu, I. Uchegbu, A. Schatzlein, J. Moger, Journal of Raman Spectroscopy, **2012**,5,681-688 .

(30) N.L. Garrett, A. Lalatsa, I. Uchegbu, A. Schatzlein, J. Moger, J. Biophotonics, **2012**, 5, 458-468.

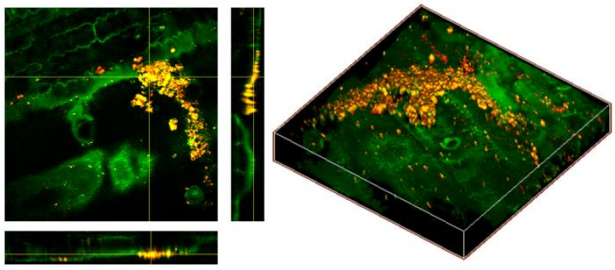

Table of contents image